

# Mapping global surface roughness using AMSR-E passive microwave remote sensing



X.Z. Chen<sup>a,b,\*</sup>, Y. Li<sup>c,1</sup>, Y.X. Su<sup>c</sup>, L.S. Han<sup>c</sup>, J.S. Liao<sup>d</sup>, S.B. Yang<sup>b</sup>

<sup>a</sup> Key Laboratory of Vegetation Restoration and Management of Degraded Ecosystems, South China Botanical Garden, Chinese Academy of Sciences, Guangzhou 510650, China

<sup>b</sup> Jiangsu Key Laboratory of Agricultural Meteorology, College of Applied Meteorology, Nanjing University of Information Science and Technology, Nanjing 210044, China

<sup>c</sup> Guangzhou Institute of Geography, Guangzhou 510070, China

<sup>d</sup> Department of Biological Sciences, University of Notre Dame, Notre Dame, IN 46556, USA

## ARTICLE INFO

### Article history:

Received 13 March 2014

Received in revised form 24 July 2014

Accepted 28 July 2014

Available online 8 August 2014

### Keywords:

Surface roughness

Physical-based retrieval model

Passive microwave remote sensing

Advanced Microwave Scanning Radiometer –

Earth Observing System (AMSR-E)

Brightness temperature ( $T_b$ )

## ABSTRACT

Surface roughness is an important geography parameter required in various research fields. Passive microwave remote sensing could be stably used for global surface roughness simulations. This paper develops a physical-based surface roughness retrieval model on the basis of the passive microwave radiative transfer equation using the C-band (6.9 GHz) and X-band (10.7 GHz) brightness temperatures of Advanced Microwave Scanning Radiometer – Earth Observing System (AMSR-E). Results show that there is a significant linear relationship between the model-derived surface roughness and that simulated by Hong (2010a) ( $R^2 = 0.62$ ; root mean square error (RMSE) = 0.09 cm). Seasonal variations of the monthly average surface roughness in 2009 indicate that vegetated lands and freezing lands are usually significantly rougher than the un-vegetated bare grounds, while snow-cover lands and deserts always have smoother surfaces than the vegetated lands. In summary, vegetation cover, freezing soil and snow cover are important factors influencing the land surface roughness conditions. It is worthy mentioning that the proposed global surface roughness retrieval model only uses AMSR-E C- and X-band brightness temperatures without any ancillary data and might be fitted for global applications.

© 2014 Published by Elsevier B.V.

## 1. Introduction

Surface roughness is a vital parameter in the pedology, agronomy, geology and hydrology research fields (Singh et al., 2000, 2003). Generally, it has two definitions. One is defined as the large-scale surface roughness that represents the surface topographic variations at length scales below the resolution of available digital elevation models or maps (Mushkin and Gillespie, 2005). Another is defined as the small-scale surface roughness, which represents the standard deviation of the surface heights that caused by soil/rock variations but not including the vegetations (Hong, 2010a). This paper refers to the latter definition. The small-scale surface roughness not only has a significant impact on infiltration and soil erosion in the agronomy and pedology processes, but also influences the ability of soil to store and release water through evaporation in hydrologic processes. In addition, Mama et al. (1997) demonstrated that surface roughness could provide useful information on explaining or distinguishing the geologic process such as eolian sand and rocky surface. Some application studies also found that remote sensing accuracy of surface soil moisture is very sensitive to surface

roughness (Dobson et al., 1985; Fung, 1994; Ulaby and Bare, 1979; Ulaby et al., 1986), which poses major problems for current soil moisture retrievals (Davidson et al., 2000; Mattia and Le Toan, 1999; Wagner et al., 2007). Therefore, it is necessary to accurately map the regional surface roughness conditions (Moran et al., 2004).

During the past 20 years, several important studies have been conducted and results have proved that passive microwave remote sensing could be stably used for global surface roughness simulations. Huang and Jin (1995) firstly employed the scattering theory of rough surface and reciprocity using both the active and passive microwave data. Then, the relationship between surface emissivity and backscattering coefficients for surfaces of various roughness degrees was derived based on the proposed scattering theory. Finally, the surface roughness variables were retrieved from the microwave emissivity using a mesh graph, which was constructed on the basis of the relationship between surface emissivity and backscattering coefficients. But the mesh graph method was a little complicated for global applications. Hong (2010a, 2010b) established an approximate relationship between the vertically and horizontally polarized reflectivities and developed a unique retrieval small-scale roughness model. Then, the global small-scale roughness over land surfaces was estimated using the 6.9 GHz brightness temperature ( $T_b$ ) of the Advanced Microwave Scanning Radiometer – Earth Observing System (AMSR-E) based on the proposed retrieval model. The small-scale roughness was retrieved within the reasonable range of previous works.

\* Corresponding author at: South China Botanical Garden, Chinese Academy of Sciences, Guangzhou 510650, China.

E-mail address: [chenxz@scbg.ac.cn](mailto:chenxz@scbg.ac.cn) (X.Z. Chen).

<sup>1</sup> Co-first author.

Hong (2010b) expanded the model and applied for retrieving the small-scale roughness over sea ices using AMSR-E  $T_b$ . Results also showed reasonable agreement with the known observations, ranging from 0.2 cm to 0.6 cm for the sea ice in the Antarctic and Arctic regions. However, Hong's method had to use other parameters such as land surface temperature as the input variable for supporting the global surface roughness simulation (Hong, 2010a). Chen et al. (2012) developed a surface roughness index using AMSR-E C-band (6.9 GHz), X-band (10.7 GHz) and L-band (18.7 GHz) Microwave Polarization Difference Index (MPDI). Results showed that the proposed surface roughness index minimized the impacts from the vegetations and was effective to map the surface roughness at both global scale and regional scale. But the empirical surface roughness index also has its defects and might bring some disadvantages when applied for time-series studies at the global scale. In summary, remote sensing of global surface roughness is still rarely studied at present. In particular, most current methods have some disadvantages: either some need variables as the input parameters or some are empirical models, which might bring unexpected errors when applied for long-time applications at the global scale. Hence, new surface roughness retrieval models are needed at the current stage.

In this paper, we aim to develop a physical-based model to map global surface roughness from AMSR-E C- and X-band  $T_b$  without any ancillary data. The proposed model is based on the passive microwave radiative transfer equation (Mo et al., 1982; Owe et al., 2001), surface roughness model (Wang and Choudhury, 1995), vegetation optical depth ( $\tau_c$ ) model (De Jeu, 2003) and MPDI (Becker and Choudhury, 1988; Choudhury and Tucker, 1987; Choudhury et al., 1987).

## 2. Materials

AMSR-E radiometer onboard the NASA Earth Observing System (EOS) Aqua satellite is a modified version of the AMSR radiometer that launched on the Japanese Advanced Earth Observing Satellite-II (ADEOS-II) in 1999. It is a conically scanning total power passive microwave radiometer sensing microwave  $T_b$  at 12 channels and 6 frequencies (6.9, 10.65, 18.7, 23.8, 36.5 and 89.0 GHz). All channels operate in both vertical (V) and horizontal (H) polarization at the incidence angle of 55.0°. The National Snow and Ice Data Center (NSIDC) has provided AMSR-E/Aqua Daily Global Quarter-Degree Gridded Brightness Temperatures data in the grid-format file, which are produced in the Equal-Area Scalable Earth Grid (EASE-Grid) at 25 km horizontal resolution in one global cylindrical, equidistant latitude–longitude projection (<http://nsidc.org/>). On October 4th, 2011, the AMSR-E radiometer reached its limit to maintain the rotation speed necessary for regular observations and automatically halted its observations and rotations. The Advanced Microwave Scanning Radiometer 2 (AMSR2) onboard the GCOM-W1 satellite has been successfully spun up, which will provide us with highly accurate measurements of the intensity of microwave emission and scattering. In the study, one-year global AMSR-E  $T_b$  data in 2009 downloaded from NSIDC are used to establish the surface roughness retrieval model.

## 3. Methods

### 3.1. Basic theory of the small-scale surface roughness model

The small-scale roughness of a material surface can be defined as W-C model (Wang and Choudhury, 1995; Wigneron et al., 2001).

$$\sigma = \frac{\lambda}{4\pi \cos\theta} \sqrt{h} \quad (1)$$

where  $\sigma$  is the small-scale surface roughness, unit: cm;  $\lambda$  is the wavelength;  $\pi$  is the circumference ratio;  $\theta$  is the incident angle of the remote sensed instrument;  $h$  represents the effective roughness height.

The reflectivity of rough surfaces can be expressed by Wang and Choudhury's Q/H surface roughness model (Wang and Choudhury, 1995).

$$r_{sv} = [(1-Q)r_{ov} + Qr_{oh}]e^{-h} \quad (2-1)$$

$$r_{sh} = [(1-Q)r_{oh} + Qr_{ov}]e^{-h} \quad (2-2)$$

where  $r_{sv}$  and  $r_{sh}$  represent the vertical polarization and horizontal polarization reflectivities of rough surfaces, respectively;  $r_{ov}$  and  $r_{oh}$  represent the vertical polarization and horizontal polarization reflectivities of flat surfaces, respectively;  $Q$  is the cross polarization ratio of surface roughness;  $h$  represents the effective roughness height. The values of  $Q$  for 6.6 GHz and 10.7 GHz frequencies simulated to equaling 0.09 and 0.11 by Njoku and Li (1999).

### 3.2. Simplification of the passive microwave radiative transfer equation

A simple atmospheric correction was firstly implemented to eliminate the atmospheric influences on AMSR-E C-band and X-band  $T_b$  using Pellarin's atmospheric correction method (Pellarin et al., 2003, 2006), which quantified globally at L-band, C-band and X-band based on the Earth Vegetation Atmosphere Model (EVA, Kerr and Njoku, 1990). The atmospheric effects for the three wavelengths are presented in Fig. 1 and Table 1. In this paper, values of 2.17 and 3.45 K are used to correct the atmosphere effects on AMSR-E C-band and X-band microwave radiations, respectively.

After the simple atmospheric correction, the atmospheric impacts on microwave emission can be ignored in the radiative transfer equation, and the radiative  $T_b$  of AMSR-E C-band and X-band is expressed as (Mo et al., 1982):

$$T_{bp} = T_s(1-r_{sp})e^{-\tau_c} + T_c(1-w_p)(1-e^{-\tau_c}) + r_{sp}T_c(1-w_p) \times (1-e^{-\tau_c})e^{-\tau_c} \quad (3)$$

where  $p$  is the horizontal (H) or vertical (V) polarization mode;  $T_{bp}$  is the brightness temperature at the  $p$  polarization mode;  $T_s$  represents the thermometric temperatures of the soil;  $r_{sp}$  is the rough-surface reflectivity;  $\tau_c$  is the optical depth of land surface vegetation;  $e^{-\tau_c}$  is the transmissivity;  $T_c$  is thermometric temperatures of the canopy;  $w_p$  is the single scattering albedo.

Many studies have demonstrated that the effects of the single scattering albedo  $w_p$  are negligible and can be ignored at low frequencies (<10 GHz, like AMSR-E C- and X-bands) (Chen et al., 2011, 2012;

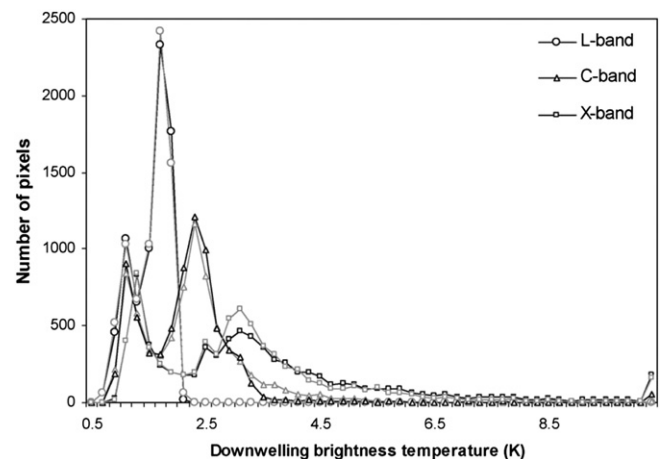


Fig. 1. Global-scale atmospheric influences on the down-welling brightness temperatures ( $T_b$ ) of microwave L, C and X-band wavelengths, respectively (Pellarin et al., 2006).

**Table 1**  
Average atmospheric contributions on C-band and X-band  $T_b$  of 1.4, 6.9 and 10.7 GHz globally (Pellarin et al., 2006).

Microwave frequency (GHz)	Average atmospheric contributions on $T_b$ (K)
1.4	1.44
6.6	2.17
10.7	2.35

Hong and Shin, 2011; Schmugge and Jackson, 1993; Wang et al., 2006). In order to derive a simple estimation model from the radiative transfer equation, we ignore the single scattering contributions on AMSR-E C-frequency (6.9 GHz) and X-frequency (10.7 GHz) and assume that the surface soil temperature  $T_s$  equals to the vegetation canopy temperature  $T_c$  (Njoku and Li, 1999; Paloscia and Pampaloni, 1988; Schmugge and Jackson, 1993; Wigneron et al., 2003; Meesters et al., 2005; Hong and Shin, 2011). Then, the passive microwave radiative transfer equation is simplified as:

$$T_{bp} = T_c(1 - r_{sp}e^{-2\tau_c}). \tag{4}$$

3.3. Development of the surface roughness retrieval model

MPDI is a classic microwave vegetation index for characterizing the land surface vegetation cover conditions (Jackson and Schmugge, 1991; Kerr and Njoku, 1990; Le Vine and Karam, 1996; Njoku and Li, 1999; Pampaloni and Paloscia, 1986). Its definition formula is described as:

$$MPDI = \frac{Tbv - Tbh}{Tbv + Tbh} \tag{5}$$

where  $Tbh$  and  $Tbv$  represent the horizontal and vertical  $T_b$ , respectively.

Substitute Eqs. (4) and (5) into Eq. (1), leading to (Wang et al., 2006):

$$\frac{1}{MPDI} = \frac{r_{ov} + r_{oh}}{(1-2Q)(r_{ov}-r_{oh})} - \frac{2}{(1-2Q)(r_{ov}-r_{oh})} e^{2\tau_c+h}. \tag{6}$$

De Jeu (2003) developed a relation (Eq. (7)) between the vegetation optical depth ( $\tau_c$ ) and MPDI on the basis Meesters'  $\tau_c$  model (Meesters

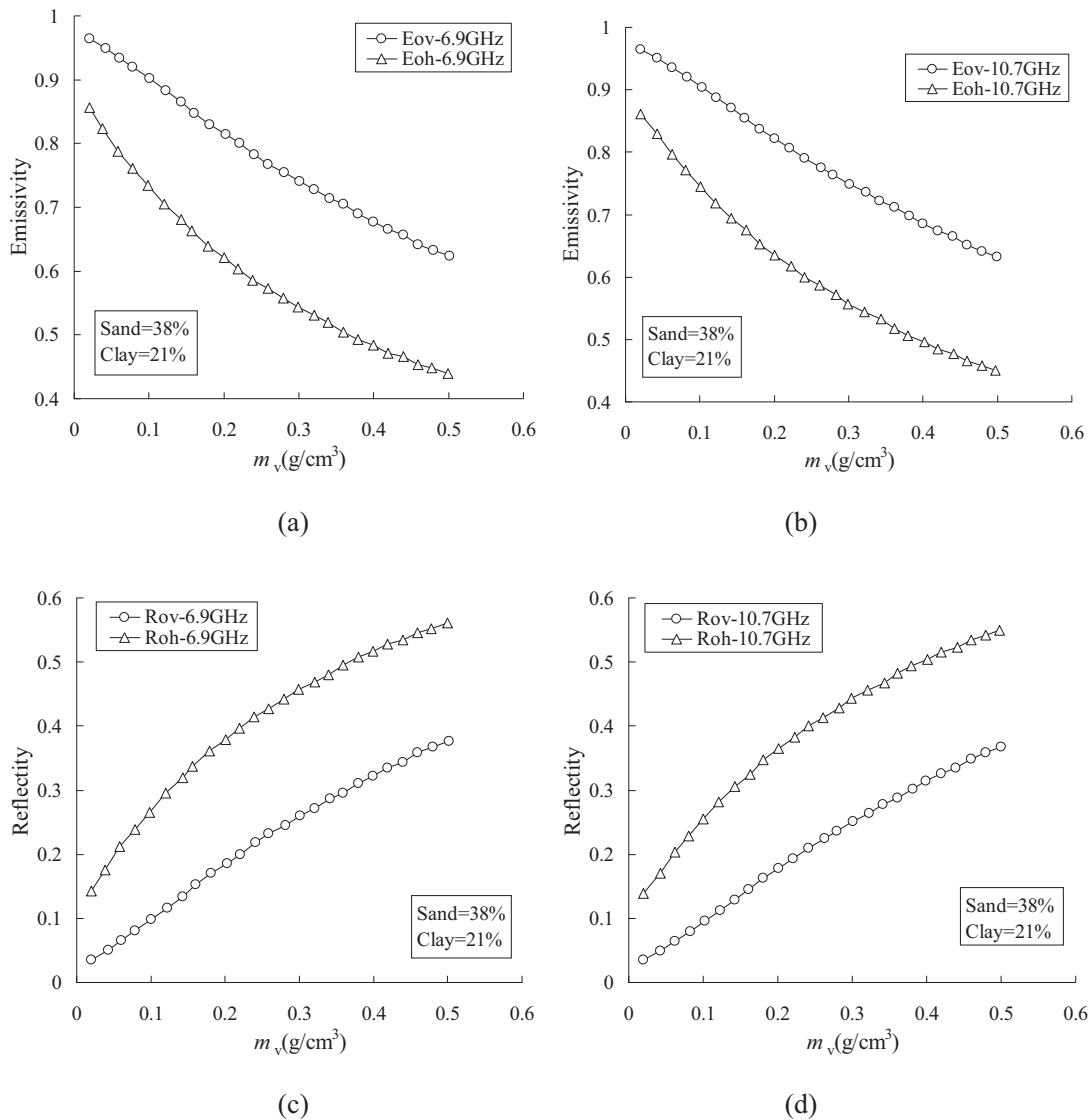


**Fig. 2.** Relations between surface soil moisture ( $m_v$ ) and soil emissivity ( $E_{op}$ ), and  $m_v$  and surface reflectivity ( $r_{op}$ ) for AMSR-E 6.9 and 10.7 GHz vertical (V) and horizontal (H) polarization channels.

**Table 2**  
Values of the parameters in the surface roughness retrieve model (Eqs. (10-1), (10-2)).

Parameters	Values
Q	0.09
α	1.2446
β	0.3586

et al., 2005). Wang et al. (2006) and Ma (2007) have proved that De Jeu's empirical solution of  $\tau_c$  held well with Wang and Choudhury's Q/H surface roughness model (Eq. (2)).

$$\tau_c = C_1 \ln(\text{MPDI})^3 + C_2 \ln(\text{MPDI})^2 + C_3 \ln(\text{MPDI}) + C_4 \quad (7)$$

where  $C_1, C_2, C_3$  and  $C_4$  are undetermined coefficients.

By substituting Eq. (7) into Eq. (6), we come to:

$$(\text{MPDI} - 1 + 2Q) \times r_{ov} + (\text{MPDI} + 1 - 2Q) \times r_{oh} = 2(\text{MPDI})^\alpha \times e^{\beta+h} \quad (8)$$

where  $\alpha = 6C_1 + 4C_2 + 2C_3, \beta = 2C_4$ . The optimal solutions for  $\alpha$  and  $\beta$  were set as 1.2446 and 0.3586 that were simulated from 1152 pairs of MPDI and surface soil moisture ( $m_v$ ) values using the Levenberg-Marquardt method (Chen et al., in press).

Further, the vertical polarization emissivity ( $E_{ov}$ ) and horizontal polarization emissivity ( $E_{oh}$ ) of AMSR-E C-band (6.9 GHz) and X-band (10.7 GHz) under different  $m_v$  from 0 g/cm<sup>3</sup> to 0.50 g/cm<sup>3</sup> were simulated using the method of Zhong (2005), shown in Fig. 2a and b. Then, the relations between  $m_v$  and  $r_{ov}, m_v$  and  $r_{oh}$  (Fig. 2c and d) are derived from the surface emissivity ( $E_{op}$ ) using the equation:  $r_{op} = 1 - E_{op}$ . Relation equations for AMSR-E C- and X-bands are listed as follows:

$$r_{ov6.9} = 0.7258 * m_v + 0.0314 (R^2 = 0.993) \quad (9-1)$$

$$r_{oh6.9} = 0.7757 m_v^{0.4481} (R^2 = 0.997) \quad (9-2)$$

$$r_{ov10.7} = 0.7117 m_v + 0.0284 (R^2 = 0.995) \quad (9-3)$$

$$r_{oh10.7} = 0.7619 m_v^{0.4610} (R^2 = 0.994) \quad (9-4)$$

where  $r_{ov6.9}$  means the flat-surface reflectivity of C-band V polarization;  $r_{oh6.9}$  means the flat-surface reflectivity of C-band H polarization;  $r_{ov10.7}$  means the flat-surface reflectivity of X-band V polarization; and  $r_{oh10.7}$  means the flat-surface reflectivity of X-band H polarization.

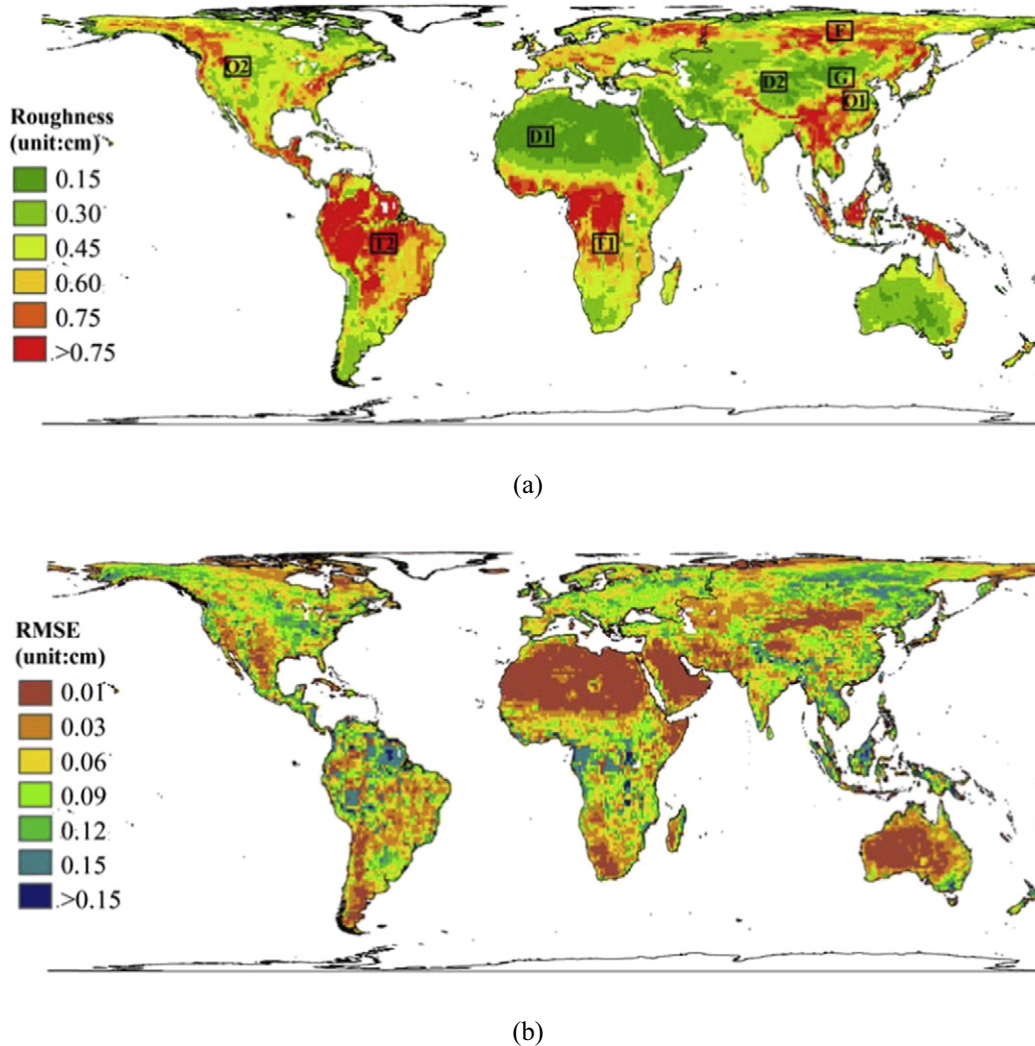


Fig. 3. Global annual average surface roughness and RMSE maps in 2009 (horizontal resolution: 25 km).

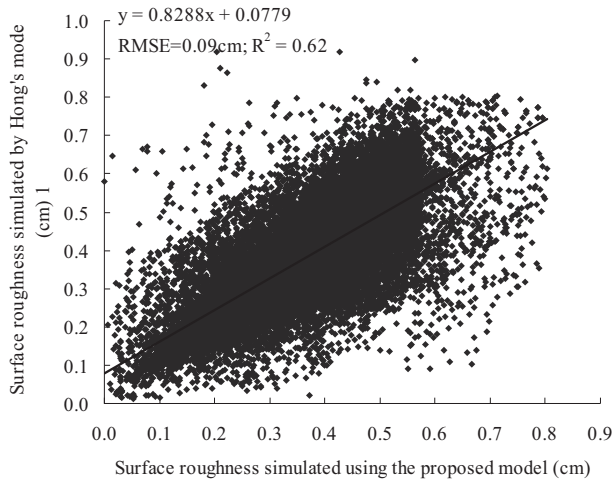


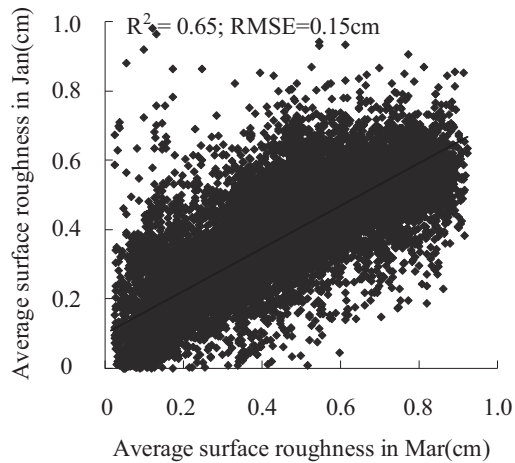
Fig. 4. Scatter diagrams between model-derived global monthly average surface roughness and those from Hong's (2010a) model in April, 2009.

Finally, the surface roughness retrieval models for AMSR-E C-band (Eq. (10-1)) and X-band (Eq. (10-2)) are established by substituting Eqs. (9-1), (9-2), (9-3), (9-4) into (8), respectively.

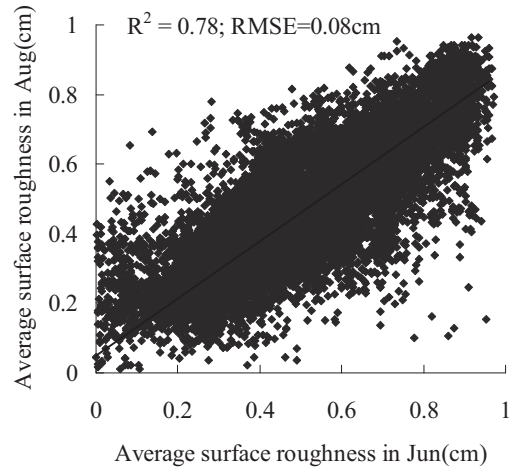
$$\begin{aligned} & (\text{MPDI}_{6.9} - 1 + 2Q) \times (0.7528 \times m_v + 0.0314) \\ & + (\text{MPDI}_{6.9} + 1 - 2Q) \times (0.7757 \times m_v^{0.4481}) \\ & = 2(\text{MPDI}_{6.9})^\alpha \times e^{\beta+h} \end{aligned} \tag{10-1}$$

$$\begin{aligned} & (\text{MPDI}_{10.7} - 1 + 2Q) \times (0.7117 \times m_v + 0.0284) \\ & + (\text{MPDI}_{10.7} + 1 - 2Q) \times (0.7619 \times m_v^{0.4610}) \\ & = 2(\text{MPDI}_{10.7})^\alpha \times e^{\beta+h} \end{aligned} \tag{10-2}$$

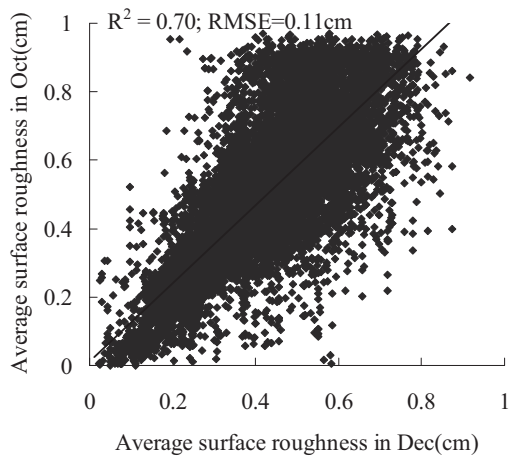
Because Eqs. (10-1) and (10-2) are two equations that contain two same variables ( $h$  and  $m_v$ ), the surface roughness parameter ( $h$ ) can be retrieved from AMSR-E C- and X-band MPDI after deleting the  $m_v$  variable by combining the two equations. Then, surface roughness ( $\sigma$ )



(a)



(b)



(c)

Fig. 5. Comparisons of the global monthly averaged surface roughness between January and March, June and August, and October and December in 2009.

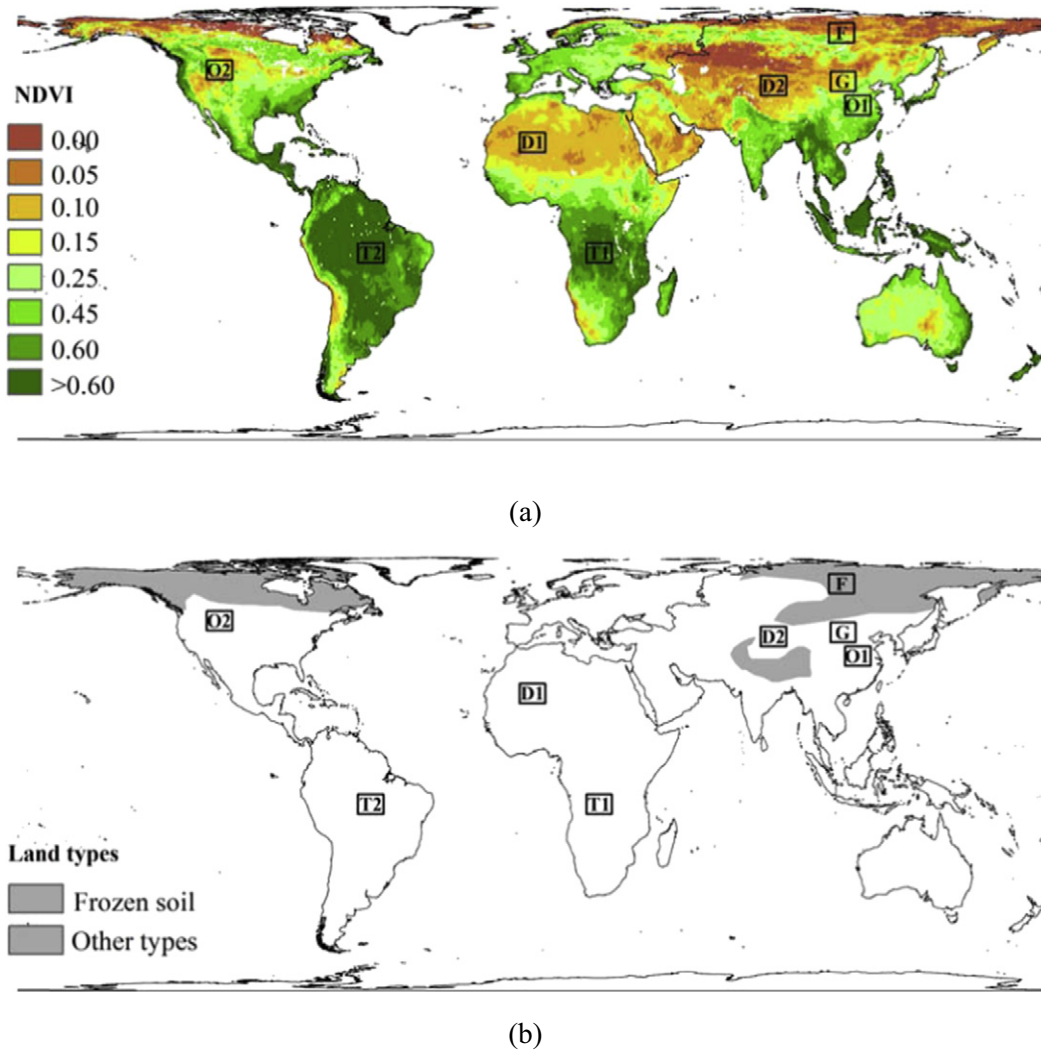


Fig. 6. The global annual mean Normalized Difference Vegetation Index (NDVI) map (horizontal resolution: 0.5 s) and freezing ground distribution map in 2009.

can be derived from  $h$  using Eq. (1). Values of the model parameters in Eqs. (10-1) and (10-2) are listed in Table 2.

4. Results and discussion

4.1. Global surface roughness mapping results and validations

The global annual average surface roughness map in 2009 is shown in Fig. 3a. The spatial horizontal resolution is 25 km as the same as that of AMSR-E  $T_p$  data. There are clearly visual correspondences that the Northern Eurasian continent, Northern Asia, Southwestern China, Central Africa, the western areas of North America, the northern areas of South America and the Eastern Australia are usually distributed with high surface roughness. While low surface roughness is mainly located at the Northern Africa, Central of Eurasian continent and Southern Australia. One-month global land surface roughness (224 168 samples in April, 2009), estimated using Hong's (2010a) method (Appendix A), is used to validate the retrieval accuracy of the proposed surface roughness model. Results show that the proposed model could effectively measure the surface roughness ranging from about 0.0 cm to 1.0 cm, which is similar as Hong's study. There is a strong linear relationship ( $R^2 = 0.62$ ;  $p < 0.001$ ) between them, with the root mean square error RMSE equals to 0.09 cm (Fig. 4). When the surface roughness of the input pixel is very high or very smooth, roughness values of neighborhood eight pixels are averaged and assigned to the input pixel. In

order to test the robustness of our global land surface roughness mapping method, a global RMSE map is also generated to show the spatial variations of the surface roughness retrieval errors (Fig. 3b). The retrieval RMSE ranges of  $<0.03$  cm, 0.03–0.06 cm, 0.06–0.09 cm and  $>0.09$  cm account for about 42%, 24.9%, 18.4%, 10.0% and 4.7% proportions of the global land areas, respectively. In other words, there is in total 85.3% of the global lands with the retrieval error smaller than 0.09 cm. There is one issue worthy mentioning here. When the vegetation cover becomes too thick for AMSR-E sensors to sense the roughness of the surface below, the retrieval model would not work well. This phenomenon has

Table 3 Land cover/land use and surface roughness conditions of the selected eight regions.

Number	Annual average NDVI	Land use types	Annual average surface roughness (cm)
D1	0.08	Desert	0.171
D2	0.03	Desert	0.188
T1	0.74	Tropical rainforest	0.664
T2	0.68	Tropical rainforest	0.867
F	0.11	Frozen soil with little vegetation cover	0.646
G	0.15	Grassland	0.292
O1	0.28	Deciduous vegetation cover	0.440
O2	0.22	Deciduous spare vegetation cover	0.472

been demonstrated in our recent studies for surface  $m_v$  and  $T_s$  simulations using AMSR-E  $T_b$  data (Chen et al., in press). A threshold value has been demonstrated that when the region's MPDI is smaller than 0.01, the vegetation cover is so dense that the microwave signals emitted by surface soils are impacted seriously when penetrated through a canopy. In other words, the AMSR-E sensors fail to sense the surface conditions effectively, which therefore leads to high retrieval errors.

#### 4.2. Spatial and seasonal variations of the global surface roughness

We further compared the global surface roughness between different months in 2009. The scatter diagrams of global monthly averaged surface roughness between January and March, June and August, and October and December are presented in Fig. 5. Results show that the land surface roughness in March is generally higher than that in January, (Fig. 5a). Similarly, the land surface roughness in October is a bit higher than that in December (Fig. 5c). However, there is little difference between the land surface roughness in June and that in August (Fig. 5b). Results indirectly indicate that seasonal land surface cover changes might probably lead to time-series variations of the surface roughness conditions. In order to reveal the potential impact factors of global land surface roughness, several regions with different vegetation covers and land surface conditions are chosen for comparisons (Fig. 6 and Table 3).

Annual variations of the monthly average surface roughness in the eight regions are shown in Fig. 7. In general, the surface roughness of vegetated lands (T1, T2, O1, O2 and G) or freezing soil (F) is significantly higher than that of un-vegetated bare ground and desert (D1 and D2) (Table 3). The Sahara Desert (D1) in Northern Africa and Taklimakan Desert (D2) in Southern China are found to be covered by low surface roughness with slight seasonal variations in the whole year. The tropical rainforests in the Congo River Basin of Western Africa and Amazon Basin (T2) of Southern America are covered by high surface roughness with slight seasonal variations. The surface roughness of grassland in the Inner Mongolian Plateau (G) and freezing soil ground in Northern Asia (F) also varies little between different months. It is perhaps because that the land surface covers and land use conditions change slightly during the whole year. Contrarily, the deciduous vegetation regions in U.S.A. (O2) and Central China (O1) vary significantly. The reason might be that land surface vegetations become thicker in spring and summer, but defoliate in autumn and become snow-covered in winter. In summary, we can infer that vegetation cover and freezing soil will cause a rougher land surface, while snow cover will smooth the land surface.

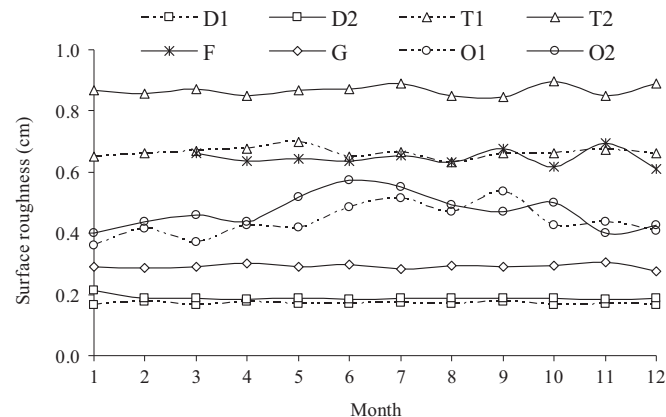


Fig. 7. Seasonal variations of monthly averaged surface roughness in 2009.

## 5. Conclusions

A global surface roughness simulation model is developed on the basis of the passive microwave radiative transfer equation using AMSR-E C- and X-band brightness temperatures. Validation results prove that the proposed surface roughness retrieval method is stable and accurate in characterizing the global land surface roughness. Analysis results indicate that vegetation cover, freezing soil and snow cover are important factors influencing the land surface roughness conditions. The surface roughness of vegetated lands or freezing grounds is significantly higher than that of un-vegetated bare grounds and deserts, while snow-cover regions always have lower surface roughness. What needs to be mentioned is that the proposed global surface roughness retrieval method only uses AMSR-E C- and X-band  $T_b$  without any ancillary data and might be fitted for global applications, but additional work using extensive in-situ data is still needed to validate the robustness of the surface roughness retrieval model.

## Acknowledgments

We are grateful to the editor and anonymous reviewers for their valuable comments and suggestions, which have greatly improved the quality of this manuscript. This study is supported jointly by Jiangsu Key Laboratory of Agricultural Meteorology (grant no. KYQ 1207), the Guangdong Science and Technology Plan Fund (grant no. 2011B020313001) and Huizhou Science and Technology Plan Fund (2013B020006005).

## Appendix A

Hong (2010a) ignored the atmospheric contributions on AMSR-E low frequencies (<10 GHz), took no consideration of volume scattering ( $\omega \approx 0$ ), assumed that the surface soil temperature  $T_s$  equals to the vegetation canopy temperature  $T_c$  and then established the following rough reflectivity  $R_r$  equation.

$$R_r = e^{2\tau_c / \cos\theta} \left(1 - \frac{T_b}{T_s}\right) \quad (\text{a1})$$

Next, Hong (2010a) developed an approximate relationship between the V-polarized and H-polarized specular surface reflectivities with the same complex refractive index and derived the small-scale roughness model (Eq. (a2)) based on the W-C reflectivity model (Wang and Choudhury, 1981).

$$\sigma = \frac{\lambda}{4\pi \cos\theta} \sqrt{\ln \left( \frac{R_{r,V} \cos^2\theta}{R_{r,H}} \right)} \quad (\text{a2})$$

Following, the empirical linear relationship (Eq. (a3)) between the V-polarized  $T_b$  at 37 GHz  $T_{b,37 \text{ GHz},V}$  and 1.25 cm  $T_s$  (De Jeu, 2003) was used to replace the  $T_s$  variable in Eq. (a1). So, small-scale roughness variable  $\sigma$  could be calculated from microwave  $T_b$  of AMSR-E low frequencies.

$$T_s = 0.861 \times T_{b,37 \text{ GHz},V} + 52.550 \quad (\text{a3})$$

## References

- Becker, F., Choudhury, B.J., 1988. Relative sensitivity of normalized difference vegetation index (NDVI) and microwave polarization difference index (MPDI) for vegetation and desertification monitoring. *Remote Sens. Environ.* 24, 297–311.
- Chen, S.S., Chen, X.Z., Chen, W.Q., Su, Y.X., Li, D., 2011. A simple retrieval method of land surface temperature from AMSR-E passive microwave data—a case study over Southern China during the strong snow disaster of 2008. *Int. J. Appl. Earth Obs. Geoinf.* 13, 140–151.

- Chen, X.Z., Chen, S.S., Zhong, R.F., Su, Y.X., Liao, J.S., Li, D., Han, L.S., Li, Y., Li, X., 2012. A semi-empirical inversion model for assessing surface soil moisture using AMSR-E brightness temperatures. *J. Hydrol.* 456–457, 1–11.
- Chen, X.Z., Su, Y.X., Li, Y., Han, L.S., Liao, J.S., 2014. Retrieving China's surface soil moisture and land surface temperature using AMSR-E brightness temperatures. *Remote Sens. Lett.* (in press).
- Choudhury, B.J., Tucker, C.J., 1987. Monitoring global vegetation using Nimbus-7 37 GHz data: some empirical relations. *Int. J. Remote Sens.* 8 (7), 1085–1090.
- Choudhury, B.J., Tucker, C.J., Golus, R.E., Newcomb, W.W., 1987. Monitoring vegetation using Nimbus-7 scanning multichannel microwave radiometer's data. *Int. J. Remote Sens.* 8 (3), 533–538.
- Davidson, M.W.J., Le Toan, T., Mattia, F., Satalino, G., Manninen, T., Borgeaud, M., 2000. On the characterization of agricultural soil roughness for radar remote sensing studies. *IEEE Trans. Geosci. Remote Sens.* 38, 630–640.
- De Jeu, R.A.M., 2003. Retrieval of Land Surface Parameters Using Passive Microwave Observations (Ph.D. Dissertation) Vrije Universiteit Amsterdam.
- Dobson, M.C., Ulaby, F.T., Hallikainen, M.T., El-Rayes, M.A., 1985. Microwave dielectric behaviour of wet soil—part II: dielectric mixing models. *IEEE Trans. Geosci. Remote Sens.* 23, 35–46.
- Fung, A.K., 1994. *Microwave Scattering and Emission Models and Their Applications*, 3. Artech House, Boston, pp. 416–430.
- Hong, S., 2010a. Global retrieval of small-scale roughness over land surfaces at microwave frequency. *J. Hydrol.* 389, 121–126.
- Hong, S., 2010b. Detection of small-scale roughness and refractive index of sea ice in passive satellite microwave remote sensing. *Remote Sens. Environ.* 114 (5), 1136–1140.
- Hong, S., Shin, I., 2011. A physically-based inversion algorithm for retrieving soil moisture in passive microwave remote sensing. *J. Hydrol.* 405, 24–30.
- Huang, X.Z., Jin, Y.Q., 1995. A simple method to estimate the soil wetness and surface roughness by using active/passive microwave data. *Remote Sens. Environ.* 53 (3), 212–214.
- Jackson, T.J., Schmugge, T.J., 1991. Vegetation effects on the microwave emission of soils. *Remote Sens. Environ.* 36, 203–212.
- Kerr, Y.H., Njoku, E.G., 1990. A semi-empirical model for interpreting microwave emission from semiarid land surfaces as seen from space. *IEEE Trans. Geosci. Remote Sens.* 28, 384–393.
- Le Vine, D.M., Karam, M.A., 1996. Dependence of attenuation in a vegetation canopy on frequency and plant water content. *IEEE Trans. Geosci. Remote Sens.* 34, 1090–1096.
- Ma, Y., 2007. Study on Soil Moisture Inversion and Application With Microwave Remote Sensing in Xinjiang. Xinjiang University, Xinjiang, pp. 45–75.
- Mama, F., Toan, T., Souyris, J.C., de Carolis, G., 1997. The effect of surface roughness on multifrequency polarimetric SAR data. *IEEE Trans. Geosci. Remote Sens.* 35, 954–966.
- Mattia, F., Le Toan, T., 1999. Back scattering properties of multi-scale rough surfaces. *J. Electromagnet. Wave* 13, 491–526.
- Meesters, A.G.C.A., De Jeu, R.A.M., Owe, M., 2005. Analytical derivation of the vegetation optical depth from the microwave polarization difference index. *IEEE Trans. Geosci. Remote Sens. Lett.* 2, 121–123.
- Mo, T., Choudhury, B.J., Schmugge, T.J., Wang, J.R., Jackson, T.J., 1982. A model for microwave emission from vegetation-covered fields. *J. Geophys. Res.* 87, 11229–11237.
- Moran, M.S., Peters-Lidard, C.D., Watts, J.M., McElroy, S., 2004. Estimating soil moisture at the watershed scale with satellite-based radar and land surface models. *Can. J. Remote Sens.* 30, 805–826.
- Mushkin, A., Gillespie, A.R., 2005. Estimating sub-pixel surface roughness using remotely sensed stereoscopic data. *Remote Sens. Environ.* 99, 75–83.
- Njoku, E.G., Li, L., 1999. Retrieval of land surface parameters using passive microwave measurements at 6–18 GHz. *IEEE Trans. Geosci. Remote Sens.* 30 (2), 79–93.
- Owe, M., Jeu, R.D., Walker, J., 2001. A methodology for surface soil moisture and vegetation optical depth retrieval using the microwave polarization difference index. *IEEE Trans. Geosci. Remote Sens.* 39 (8), 1643–1654.
- Paloscia, S., Pampaloni, P., 1988. Microwave polarization index for monitoring vegetation growth. *IEEE Trans. Geosci. Remote Sens.* 26 (5), 617–621.
- Pampaloni, P., Paloscia, S., 1986. Microwave emission and plant water content: a comparison between field measurements and theory. *IEEE Trans. Geosci. Remote Sens.* 6, 900–905.
- Pellarin, T., Wigneron, J.P., Calvet, J.C., Berger, M., Douville, H., Ferrazzoli, P., Kerr, Y.H., Lopez-Baeza, H., Pulliainen, J., Simmonds, L.P., Waldteufel, P., 2003. Two-year global simulation of L-band brightness temperatures over land. *IEEE Trans. Geosci. Remote Sens.* 41 (9), 2135–2139.
- Pellarin, T., Kerr, Y.H., Wigneron, J.P., 2006. Global simulation of brightness temperatures at 6.6 and 10.7 GHz over land based on SMMR data set analysis. *IEEE Trans. Geosci. Remote Sens.* 44 (9), 2492–2505.
- Schmugge, T.J., Jackson, T.J., 1993. Passive microwave remote sensing of soil moisture. *Adv. Remote Sens.* 2 (2), 5–14.
- Singh, D., Yamaguchi, Y., Yamada, H., 2000. Response of microwave on bare soil moisture and surface roughness by X-band scatterometer. *IEEE Trans. Geosci. Electron.* E83-B (9), 2038–2043.
- Singh, D., Singh, K.P., Herlin, I., Sharma, S.K., 2003. Ground-based scatterometer measurements of periodic surface roughness and correlation length for remote sensing. *Adv. Space Res.* 32 (11), 2281–2286.
- Ulaby, F.T., Bare, J.E., 1979. Look direction modulation function of the radar backscattering coefficient of agricultural fields. *Photogramm. Eng. Remote Sens.* 45, 1495–1506.
- Ulaby, F.T., Moore, R.K., Fung, A.K., 1986. *Microwave Remote Sensing: Active and Passive*, 3. Artech House, Boston, pp. 42–48.
- Wagner, W., Blöschl, G., Pampaloni, P., Calvet, J.C., Bizzarri, B., Wigneron, J.P., Kerr, Y., 2007. Operational readiness of microwave remote sensing of soil moisture for hydrologic applications. *Nord. Hydrol.* 38, 1–20.
- Wang, J.R., Choudhury, B.J., 1981. Remote sensing of soil moisture content, over bare field at 1.4 GHz frequency. *J. Geophys. Res.* 86 (C6), 5527–5282.
- Wang, J.R., Choudhury, B.J., 1995. Passive microwave radiation from soil: examples of emission models and observations. In: Choudhury, B., Kerr, Y., Njoku, E., Pampaloni, P. (Eds.), *Passive Microwave Remote Sensing of Land-Atmosphere Interactions*. VSP, Utrecht, The Netherlands.
- Wang, L., Li, Z., Chen, Q., 2006. New calibration method for soil roughness parameters with AMSR-E observations. *J. Remote Sens.* 10 (5), 656–660 (Chinese journal).
- Wigneron, J.P., Laguerre, L., Kerr, Y.H., 2001. A simple parameterization of the L-band microwave emission rough agricultural soil. *IEEE Trans. Geosci. Remote Sens.* 39 (8), 1697–1707.
- Wigneron, J.P., Calvet, J.C., Pellarin, T., Van de Griend, A.A., Berger, M., Ferrazzoli, P., 2003. Retrieving near-surface soil moisture from microwave radiometric observations: current status and future plans. *Remote Sens. Environ.* 85, 489–506.
- Zhong, R.F., 2005. *Microwave Radiometer Carried by Shenzhou IV Data Processing and Land Surface Parameters Retrieval* (Doctoral dissertation) Institute of Remote Sensing Applications, Chinese Academy of Sciences, Beijing (in Chinese).